Report

on

Data Analysis for the Pioneer Venus Electric Field Detector

NASA Grant NAG 2-485

September 26th, 1990 - March 25th, 1991

Introduction

This report covers the interval September 26th, 1990 to March 25th 1991. In this time we have carried out research on plasma waves observed in the ion foreshock at Venus, and on the impulsive bursts observed in the nightside ionosphere. Here we will describe some results from the ion foreshock study, from a study of wave polarization, and from a study of the dependence on magnetic field orientation. We will also present an analysis of data acquired using 4096 BPS data.

Much of the analysis described here was presented at the 1990 Fall AGU Meeting in San Francisco, and at the Pioneer Venus SSG, held at NASA/Ames, in March 1991.

Plasma Waves in the Ion Foreshock

As part of our ongoing analysis of plasma waves at Venus, graduate student Gregory K. Crawford has started to analyze plasma waves observed in the ion foreshock. Some examples of the wave data are shown in Figures 1 and 2. In Figure 1 we show wave data acquired near the nose of the bow shock. The data have been filtered to remove the characteristic

interference observed when the spacecraft is in sunlight. In this area the plasma waves appear to be somewhat impulsive and relatively broad-band in nature. Throughout the interval the angle between the shock normal and the magnetic field (theta-bn) is at or slightly less than 45 degrees. In this region the shock is quasi-parallel, and we expect ions to be streaming back from the shock. These ions may be responsible for the plasma waves.

Figure 2 shows wave data acquired from the flanks of the bow shock. The wave data are qualitatively different than those shown in Figure 1. In particular, the 5.4 kHz channel is more intense, and the signal is relatively continuous. Again there is a theta-bn dependence, in that the waves are not observed for theta-bn greater than 45 degrees. This theta-bn dependence is emphasized in Figure 3, where the data are plotted both as a scatter plot and as median values in three degree bins. As for the sub-solar region, the waves are only observed for quasi-parallel shocks.

Since the waves are observed upstream of the quasi-parallel shock, both examples of data appear to be associated with ions backstreaming from the shock. However, the different quality of the waves suggests that the distribution function of the backstreaming ions may be different in the different regions. We hope to explore in more detail the properties of the waves in the ion foreshock, and perhaps gain some insight into the ion distribution function. For example, are the ions beam-like or diffuse in velocity space?

Polarization of 100 Hz waves in the Nightside

If the 100 Hz waves observed in the nightside ionosphere of Venus are due to atmospheric lightning, then they must propagate in the whistler-mode. One test for this is the polarization of wave electric field. The electric field is polarized perpendicularly to the ambient magnetic field for whistler waves. Since the signals themselves are impulsive in nature, and rarely last for a full spin of the spacecraft (~ 12 seconds), we do not often observe a clear double-lobed radiation pattern that would be expected for a spinning antenna. Consequently, we must resort to statistical analysis to overcome the aliassing inherent in sampling a short duration signal occurring at arbitrary spin phases.

Figure 4 shows three polarization plots from orbit 526. The crosses show the 100 Hz wave power as a function of spin phase, while the line labelled "B" gives the average magnetic field direction on the spin plane, and the line labelled "E" gives the maximum variance direction, which we assume is the direction of the wave electric field. The top two panels show waves that are perpendicularly polarized, and are presumably whistler-mode. The bottom panel shows an interference signal often observed on the nightside. This signal is highly polarized and will bias any statistical study of the polarization.

In order to perform statistics on the data we have analyzed all of the season 3 nightside data in 30 second intervals. We have generated a data base consisting of various parameters, such as the magnetic field direction, the maximum variance direction, and the position of the spacecraft. Because of the presence of interference signals, such as

those shown at the bottom of Figure 4 we find that the data must be "cleaned". We have removed from the data base any signals which are contaminated by interference. Results of the statistics are shown in Figure 5. The large panel at the left of the figure shows a histogram of the relative phase between "E" and "B" for a sub-set of the cleaned data. These data are those for which the magnetic field is nearly vertical and whistler-mode propagation is allowed (i.e. the wave vector is inside the resonance cone). These waves appear to be mainly perpendicularly polarized and are likely to be whistler-mode waves.

Dependence of 100 Hz Bursts on Magnetic Field Orientation

As already alluded to in the previous section, if the 100 Hz emissions in the nightside ionosphere are due to atmospheric lightning, then the orientation of the magnetic field may control the rate of occurrence of the signals. Since the refractive index in the ionosphere is so high, any signals propagating from the atmosphere through the ionosphere will have their wave vector orientated along the normal to the density gradient, through Snell's law. Whistler-mode waves are only allowed to propagate in a restricted range of angles with respect to the magnetic field. The most oblique waves propagate along a cone known as the resonance cone. The higher the wave frequency, the narrower is this cone angle. So if the magnetic field were to be perpendicular to the ionospheric density gradient then 100 Hz waves could not propagate as whistler-mode waves.

Graduate student Chang-Ming Ho has begun to study this, and some results are shown in Figure 6. This figure shows the burst rate as a

function of altitude for waves observed when the wave vector is inside or outside of the resonance cone, assuming vertical propagation (i.e. the ionosphere is horizontally stratified). Even though the magnetic field orientation is such that most of the time the waves would be outside of the resonance cone, more bursts occur when the field is inside the resonance cone, and the burst rate inside is much higher. In addition, the scale height for waves inside the resonance cone is larger than for waves outside. This appears to support the conclusion that at least some of the wave bursts are whistler-mode waves generated from an atmospheric source.

As further evidence that the 100 Hz waves are whistler-mode waves, Figure 7 shows the burst rate for 100 Hz waves as a function of the angle between the magnetic field and the radius vector (theta-br). The burst rate is a maximum when theta-br is near zero, as might be expected for whistler-mode waves. It is important to note that we have not selected the data by magnetic field orientation, it is an intrinsic property of the waves that the burst rate is maximum for parallel propagation.

Since the angle between the magnetic field and the spacecraft velocity vector is not independent of the angle with respect to the radius vector when the spacecraft is near periapsis, we also find that the burst rate maximizes when theta-bv is near 90 degrees. However, if we compute the burst rate as both a function of theta-br and theta-bv (Figure 8), then we see that the theta-br dependence dominates. At a fixed theta-br, there is little or no dependence on theta-bv. This

argues against Doppler-shift of ion acoustic waves as an explanation for the wave signatures.

High Resolution Data

Near the beginning of 1990 we requested that the Pioneer Venus project operate the spacecraft at 4096 BPS during some nightside periapsis passes. We have presented some preliminary analysis of the data at both the SSG's and in previous status reports. In those reports we emphasized the quality of the telemetry stream, with attention to the amount of data lost due to low signal to noise. Here we will describe some analysis of the signals observed at high data rates.

Figure 9 shows five minutes of high resolution data. There are several bursts in the data, which are marked with asterisks. One of the first questions we wish to address with the high rate data is if the signals show any broadening or other changes in their temporal properties, which may help in identifying the source location of the signals. However, before doing this, we want to point out that 4096 BPS data do allow us to study the detailed structure of the signals. Figure 10 shows a single event. At this high resolution, the event has some structure which may be evidence for dispersion.

One way of determining if there is any change in the temporal structure of the bursts is to determine the distribution of burst duration. This is shown in Figure 11. We calculate the burst duration by adding together the amount of time over which bursts occur at successive data points. At left of Figure 11 we compare the distribution of bursts

for 4096 BPS data and for season 3. The data from season 3 were acquired at 2048 BPS (1/4 sec) at low altitude (<300 km), while the 4096 BPS data were acquired near 1500 km altitude. In order to perform a direct comparison, however, we must convert the 4096 BPS data to an equivalent 2048 BPS resolution. this is done by adding pairs of bins together, giving the histogram at right. Within statistical uncertainty it appears that the histograms are essentially the same.

In addition to the duration we can determine the separation between bursts. This is shown in Figure 12. We again show the histogram for each data resolution at left, with the equivalent 2048 BPS data at right. However, unlike the duration statistics were bins are added together, we must take into account the probability that a pair of bursts separated by 1/8 second will be resolved at 1/4 second. It can be shown that this probability is 50%, and so half of the bursts in the first bin at 4096 are not counted for the histogram at the right. Again we find that the histograms are essentially the same.

On the one hand, the data in Figures 11 and 12 seem to suggest that there is no difference between the 2048 BPS and 4096 BPS data. However, the figures also show that if all the data were acquired at 2048 BPS then we would not be able to resolve any differences as a function of altitude. In doing the comparison we had to degrade the resolution of the 4096 BPS data, and hence loose information. We would therefore encourage the project to acquire 4096 BPS data were possible, provided there are no serious impacts on spacecraft operation.

Publications (9/26/90 - 3/25/91)

Intriligator, D.S., L.H. Brace, S.H. Brecht, W.C. Knudsen, F.L. Scarf, R.J. Strangeway, and H.A. Taylor, Jr., Evidence for unusually high densities of plasma in the Venusian ionosheath, *Geophys. Res. Lett.*, *18*, 61, 1991.

Strangeway, R.J. Plasma Waves at Venus, *Space Sci. Rev.*, *55*, 275, 1991.

Perez-de-Tejada, H., D.S. Intriligator, and R.J. Strangeway, Steady-state transition in the Venus ionosheath, *Geophys. Res. Lett.*, *18*, 131, 1991.

Crawford, G.K., R.J. Strangeway, and C.T. Russell, Variations in plasma wave intensity with distance along the electron foreshock boundary at Venus, in press, *Adv. Space Res.*, 1991.

Russell, C.T., and R.J. Strangeway, Venus lightning: an update, submitted, *Adv. Space Res.*, 1991.

Ho, C.-M., R.J. Strangeway, and C.T. Russell, Occurrence characteristics of VLF bursts in the nightside ionosphere of Venus, submitted, *J. Geophys. Res.*, 1991.

Presentations (9/26/90 - 3/25/91)

Sonwalkar, V.S., D.L. Carpenter, and R.J. Strangeway, On the question of lightning at Venus, *EOS, Trans. AGU*, *71*, 1431, American Geophysical Union Fall Meeting, San Francisco, 1990.

Strangeway, R.J., C.T. Russell, and C.-M. Ho, Whistler mode waves in the night ionosphere of Venus: lightning or in situ instabilities, *EOS, Trans. AGU*, *71*, 1431, American Geophysical Union Fall Meeting, San Francisco, 1990.

Crawford, G.K., R.J. Strangeway, C.T. Russell, and J.D. Mihalov, Investigation of plasma wave observations in the ion foreshock of Venus, *EOS, Trans. AGU*, *71*, 1515, American Geophysical Union Fall Meeting, San Francisco, 1990.

Figure Captions

Fig. 1. Example of the broad-banded wave observed in the sub-solar ion foreshock.

Fig. 2. Example of waves observed near the flank bow shock.

Fig. 3. The dependence of the 5.4 kHz wave intensity on theta-bn.

Fig. 4. Examples of nightside 100 Hz burst polarization.

Fig. 5. A statistical determination of the wave polarization, showing predominantly perpendicular polarization.

Fig. 6. Burst rate for 100 Hz waves as a function of altitude, for bursts inside and outside the whistler-mode resonance cone.

Fig. 7. 100 Hz burst rate as a function of the angle between the magnetic field and the radius vector.

Fig. 8. 100 Hz burst rate as a function of the angel between the magnetic field and the radius vector, and the spacecraft velocity vector.

Fig. 9. Example of 1/8 sec (4096 BPS) data, showing bursts observed at high altitudes in the nightside.

Fig. 10. A high resolution plot of an individual burst showing some of the detailed structure.

Fig. 11. A comparison of 100 Hz burst duration at different data rates.

Fig. 12. A comparison of 100 Hz burst separation at different data rates.

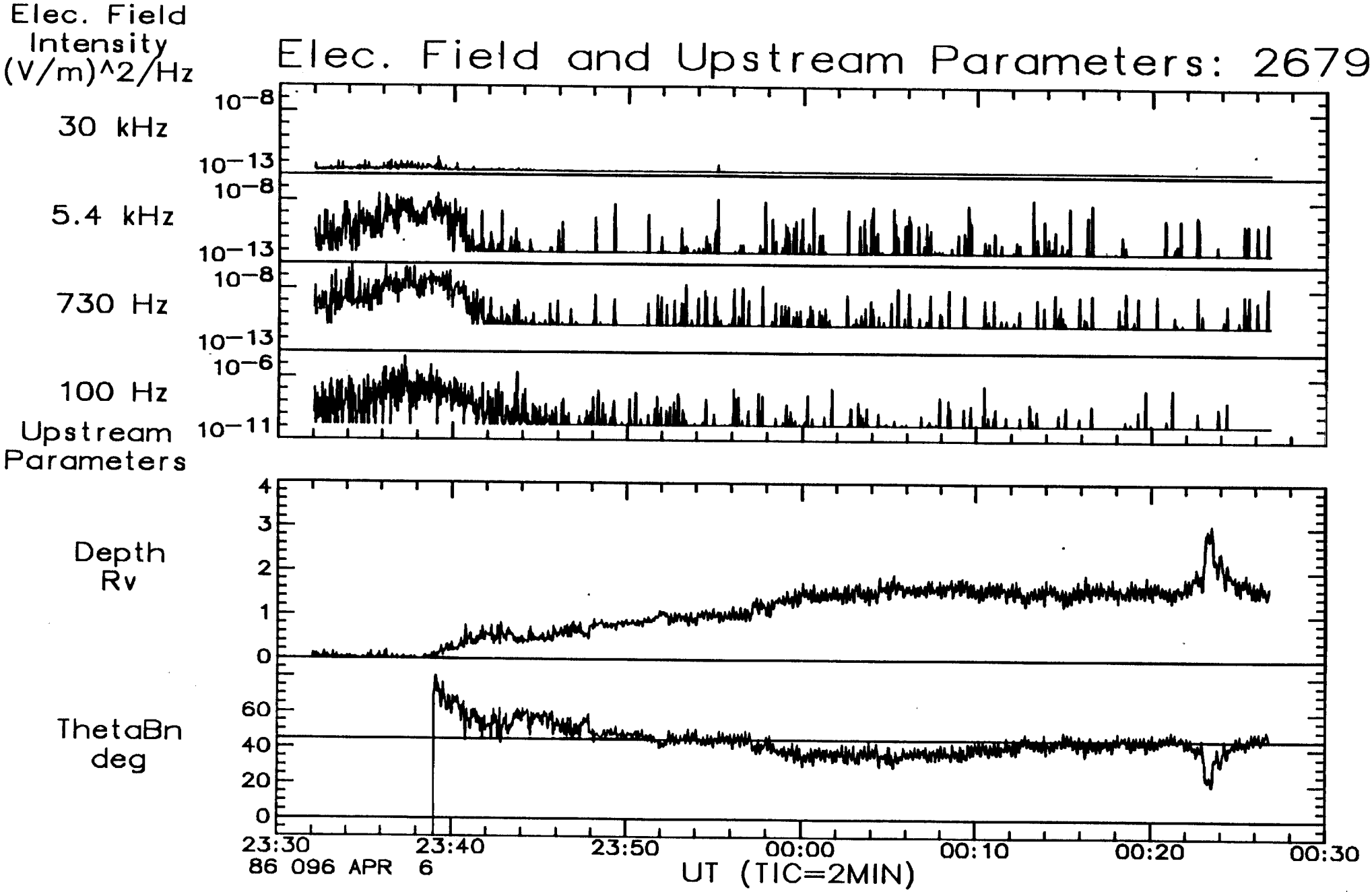
Elec. Field and Upstream Parameters: 2679
Elec. Field Intensity (V/m)^2/Hz
30 kHz
5.4 kHz
730 Hz
100 Hz
Upstream Parameters
10^-8
10^-13
10^-6
10^-11
Depth Rv
ThetaBn deg
4
3
2
1
0
60
40
20
0
23:30
23:40
23:50
00:00
00:10
00:20
00:30
86 096 APR 6
UT (TIC=2MIN)

Figure 1

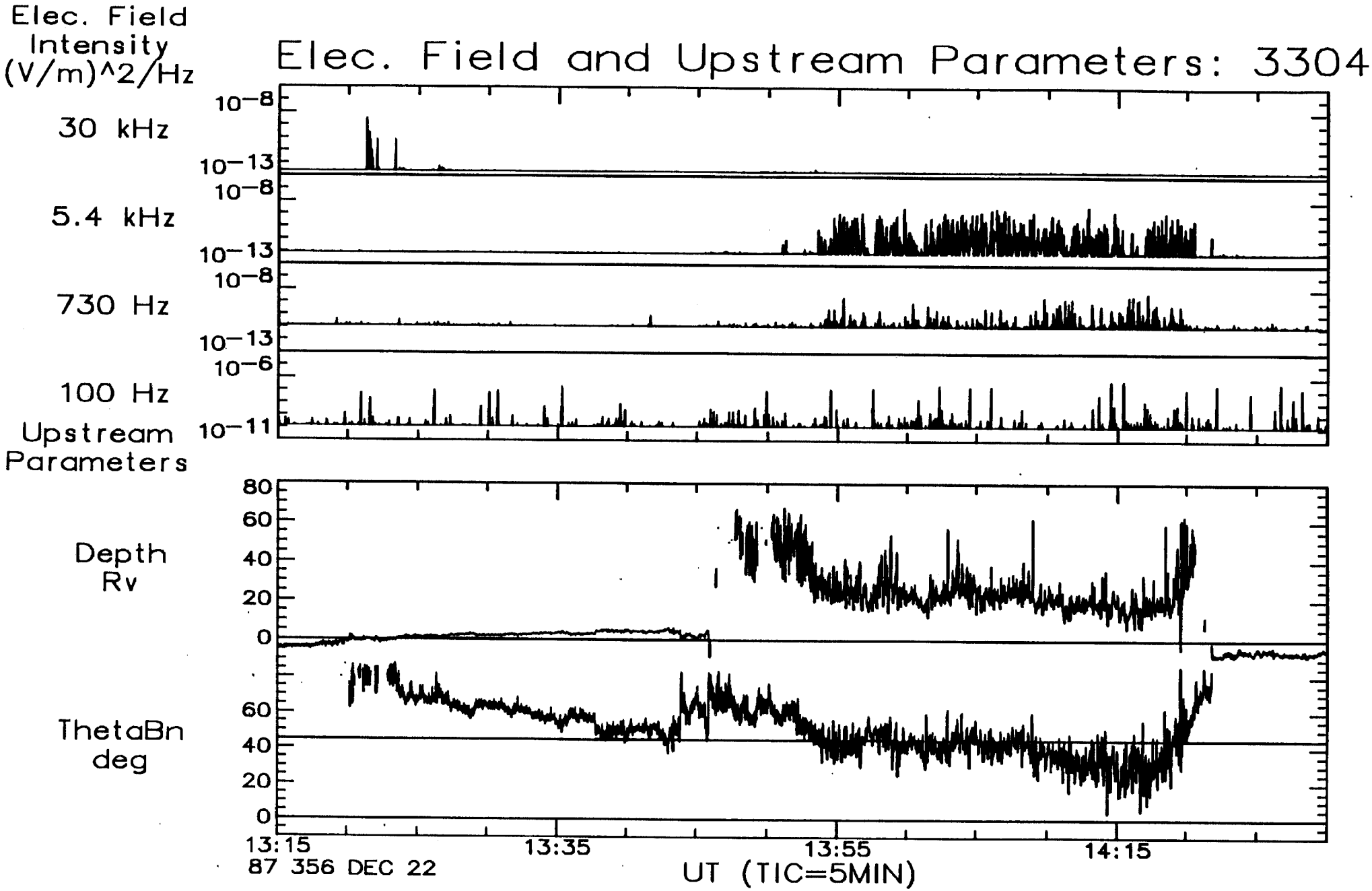
Elec. Field and Upstream Parameters: 3304
Elec. Field Intensity (V/m)^2/Hz
30 kHz
5.4 kHz
730 Hz
100 Hz
Upstream Parameters
10^-8
10^-13
10^-6
10^-11
Depth Rv
ThetaBn deg
80
60
40
20
0
13:15
13:35
13:55
14:15
87 356 DEC 22
UT (TIC=5MIN)

Figure 2

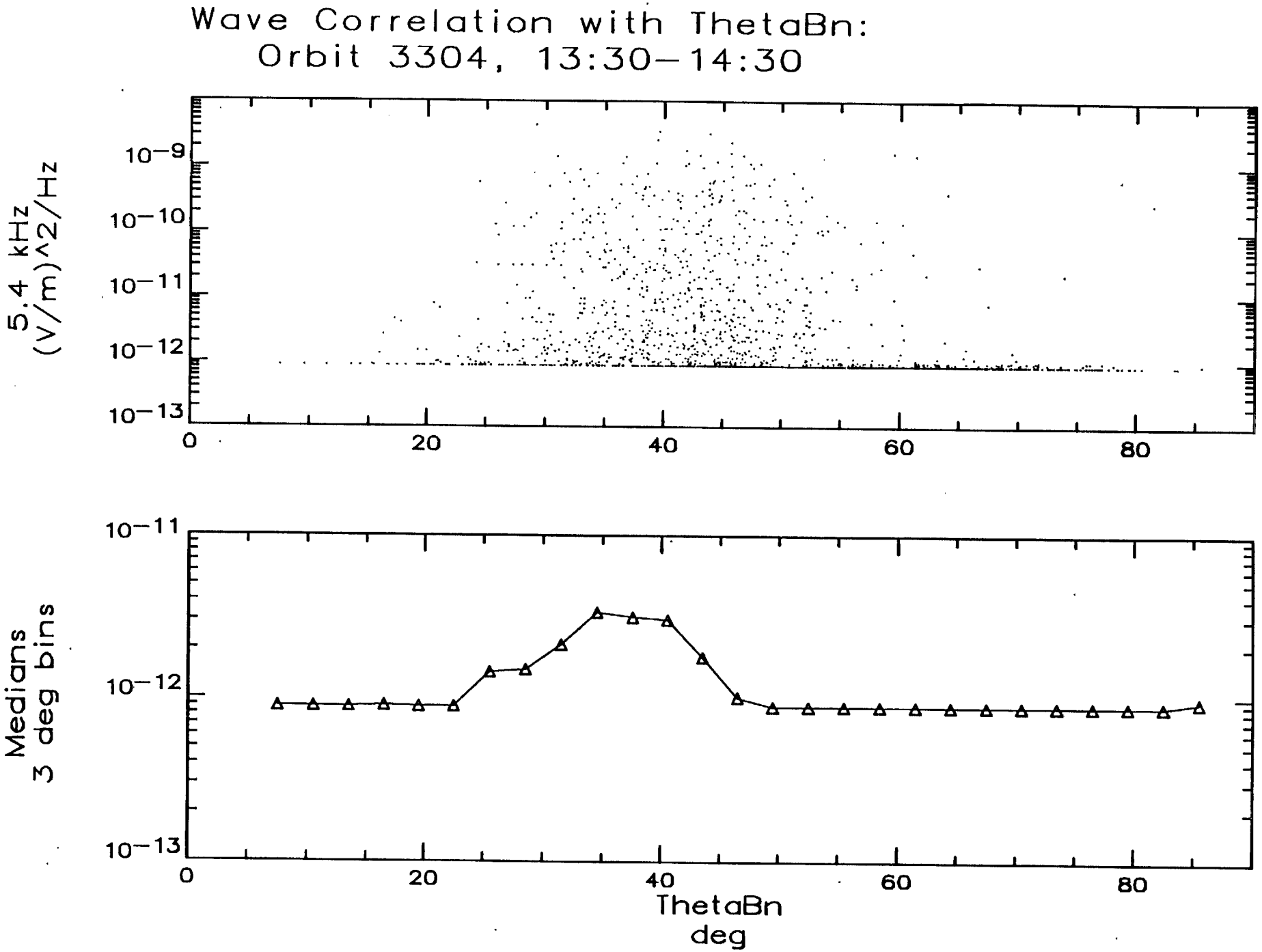
Wave Correlation with ThetaBn:
Orbit 3304, 13:30–14:30
5.4 kHz
(V/m)^2/Hz
10^-9
10^-10
10^-11
10^-12
10^-13
0
20
40
60
80
Medians
3 deg bins
10^-11
10^-12
10^-13
0
20
40
60
80
ThetaBn
deg

Figure 3

100 Hz, log $(V/m)^2/Hz$
Relative scale:
Min=5.8e-11
Max=6.7e-09
Median Ratio:
Mpar/Mper= 0.779
Variance Ratio:
Smax/Smin= 1.550
Rel angle= -76.1

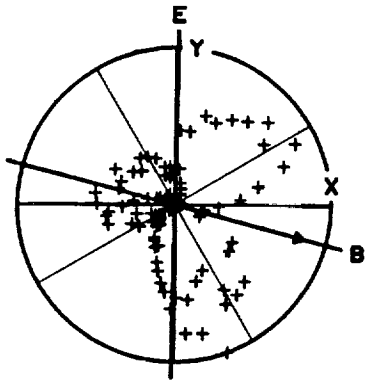

Pioneer Venus Orbit 526
80 135 May 14
09:26:30 - 09:27:00
Spectral Power vs. Phase

100 Hz, log $(V/m)^2/Hz$
Relative scale:
Min=6.3e-11
Max=2.0e-08
Median Ratio:
Mpar/Mper= 1.133
Variance Ratio:
Smax/Smin= 1.623
Rel angle= -84.6

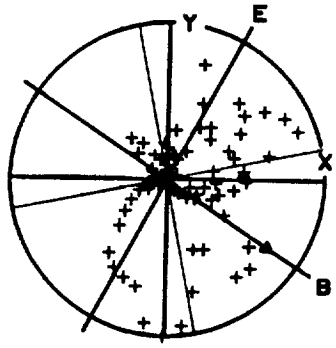

Pioneer Venus Orbit 526
80 135 May 14
09:28:00 - 09:28:30
Spectral Power vs. Phase

100 Hz, log $(V/m)^2/Hz$
Relative scale:
Min=7.5e-11
Max=5.7e-09
Median Ratio:
Mpar/Mper= 1.000
Variance Ratio:
Smax/Smin=12.708
Rel angle= -39.4

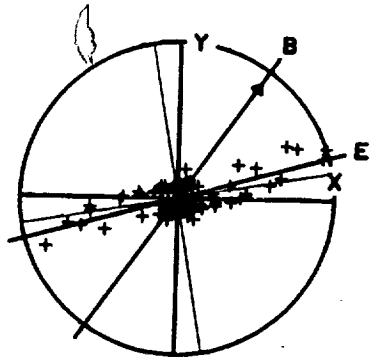

Pioneer Venus Orbit 526
80 135 May 14
09:30:30 - 09:31:00
Spectral Power vs. Phase

Figure 4

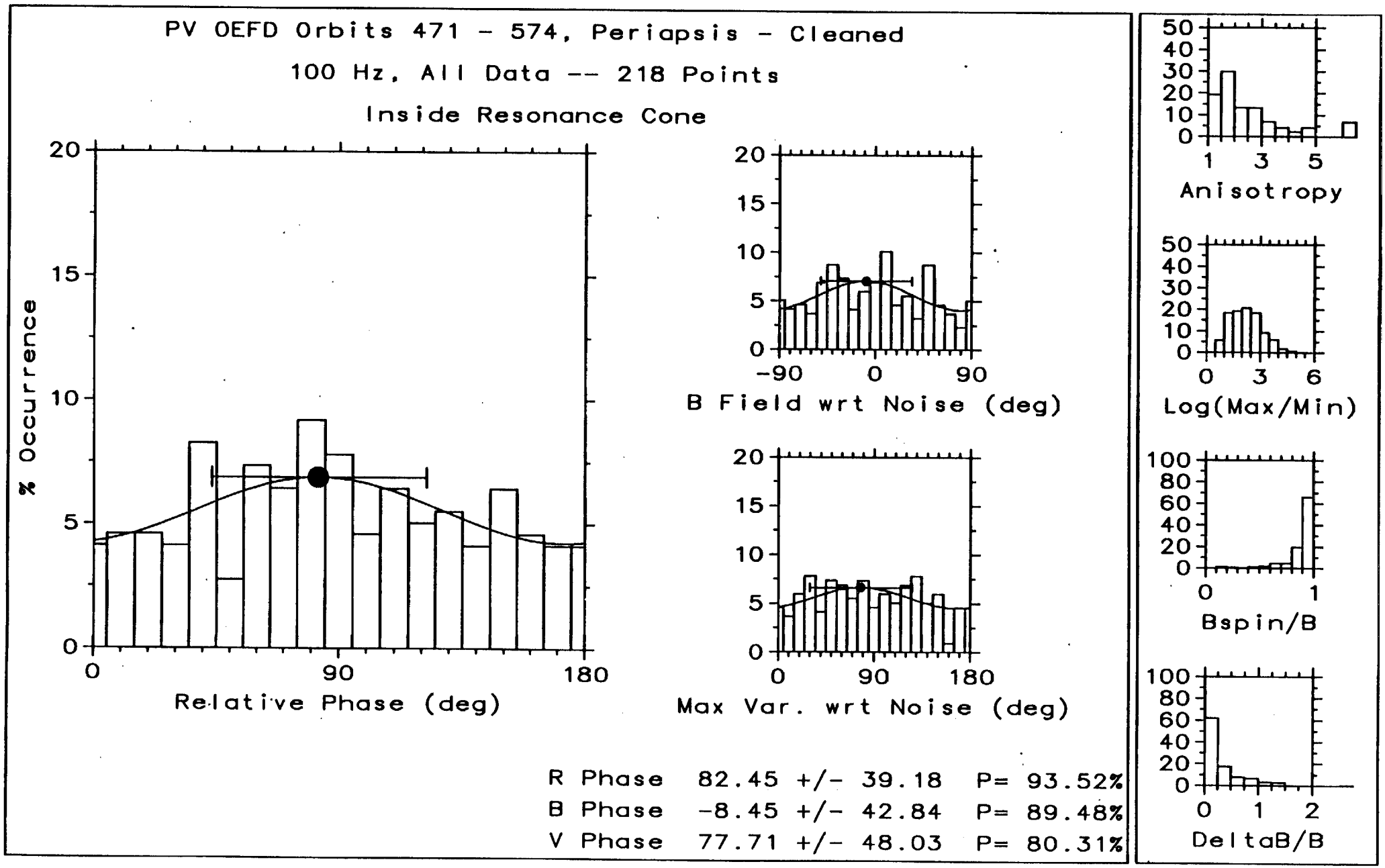
PV OEFD Orbits 471 - 574, Periapsis - Cleaned
100 Hz, All Data -- 218 Points
Inside Resonance Cone
% Occurrence
Relative Phase (deg)
B Field wrt Noise (deg)
Max Var. wrt Noise (deg)
Anisotropy
Log(Max/Min)
Bspin/B
DeltaB/B
R Phase 82.45 +/- 39.18 P= 93.52%
B Phase -8.45 +/- 42.84 P= 89.48%
V Phase 77.71 +/- 48.03 P= 80.31%

Figure 5

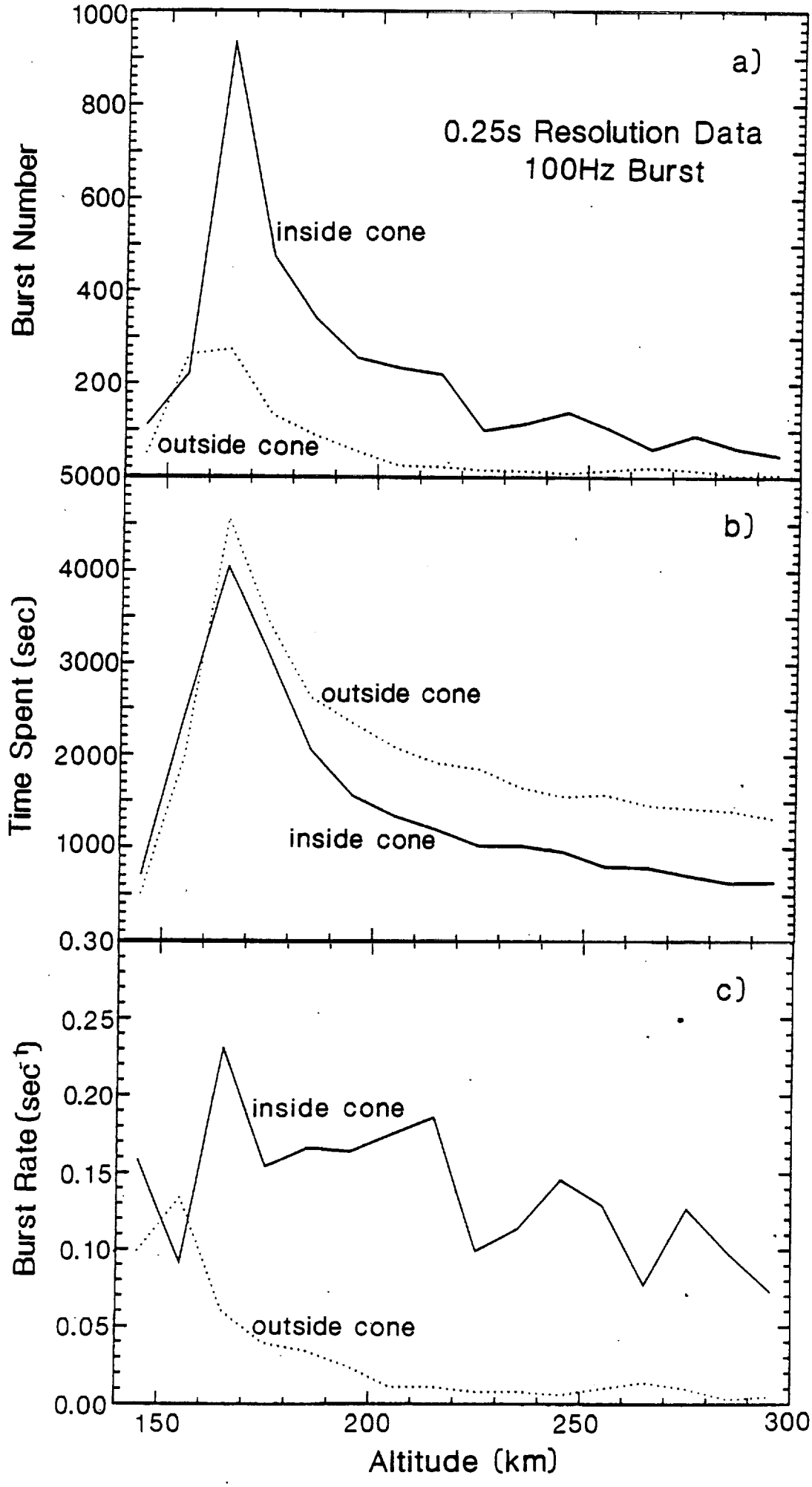
a)
0.25s Resolution Data
100Hz Burst
Burst Number
1000
800
600
400
200
5000
inside cone
outside cone
b)
Time Spent (sec)
4000
3000
2000
1000
0.30
outside cone
inside cone
c)
Burst Rate (sec⁻¹)
0.25
0.20
0.15
0.10
0.05
0.00
inside cone
outside cone
150
200
250
300
Altitude (km)

Figure 6

Burst rate as a function of θ_{br}

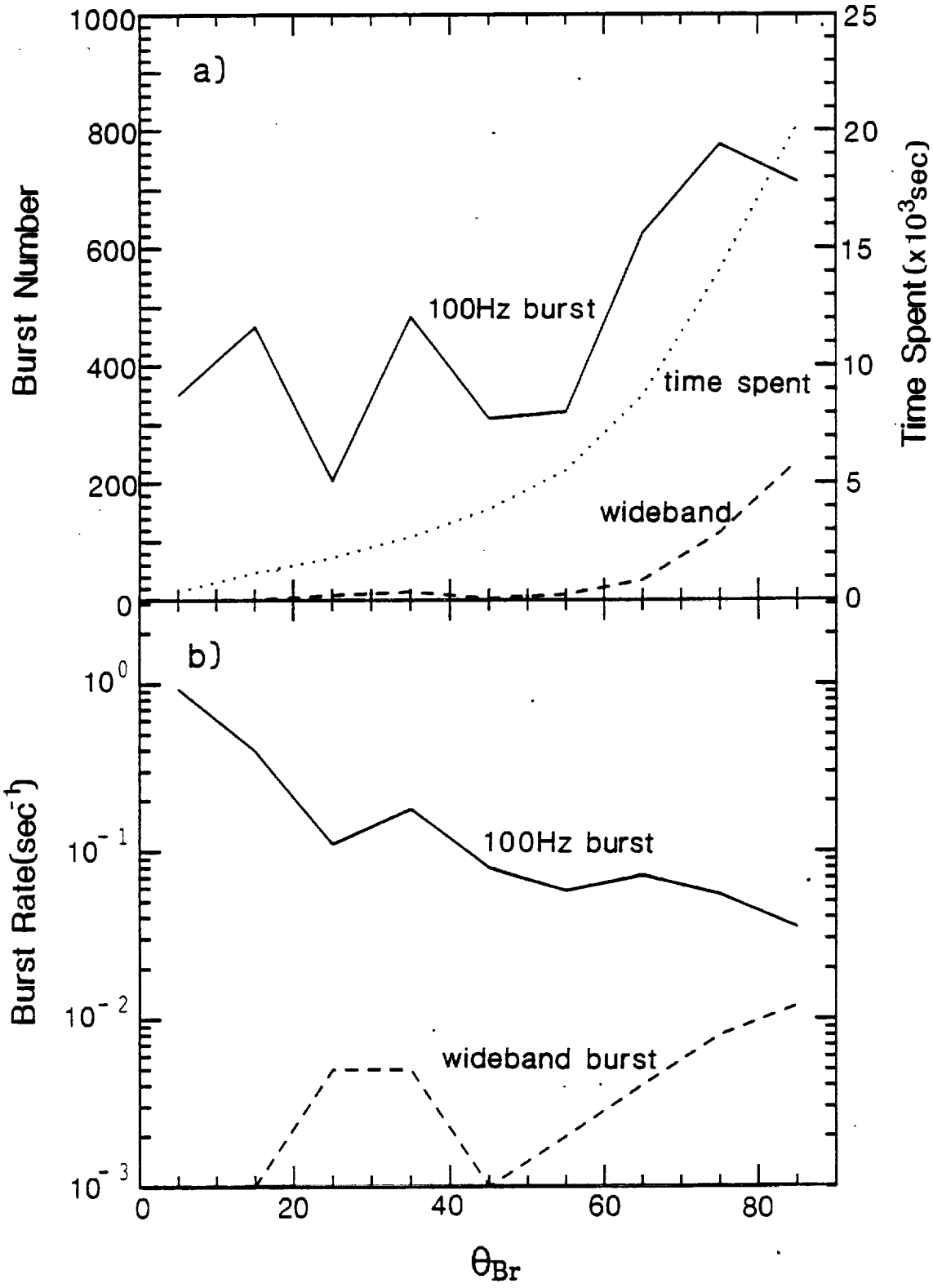

Figure 7

100Hz burst rate as a function of θ_{br} and θ_{bv} angles

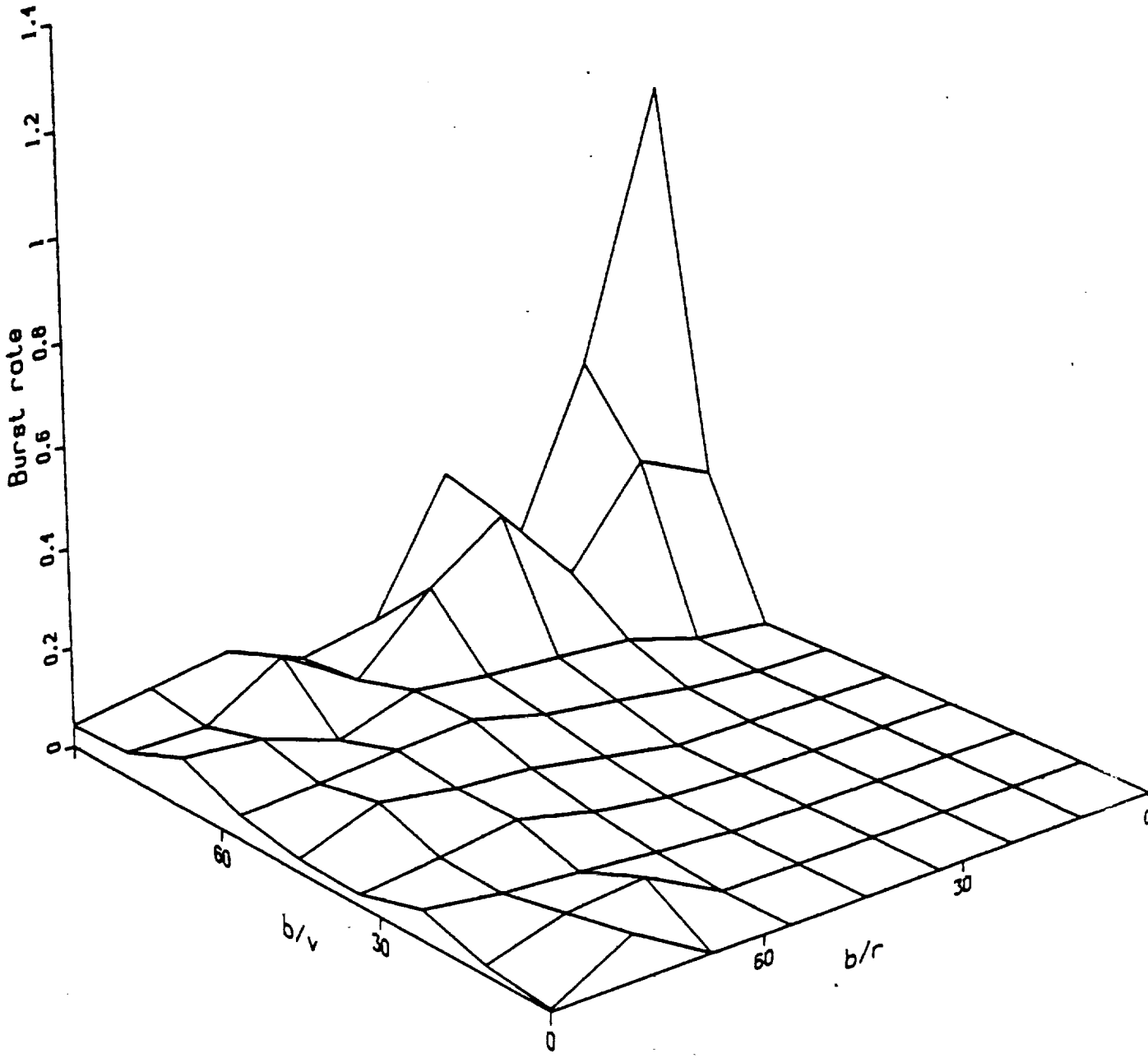

Figure 8

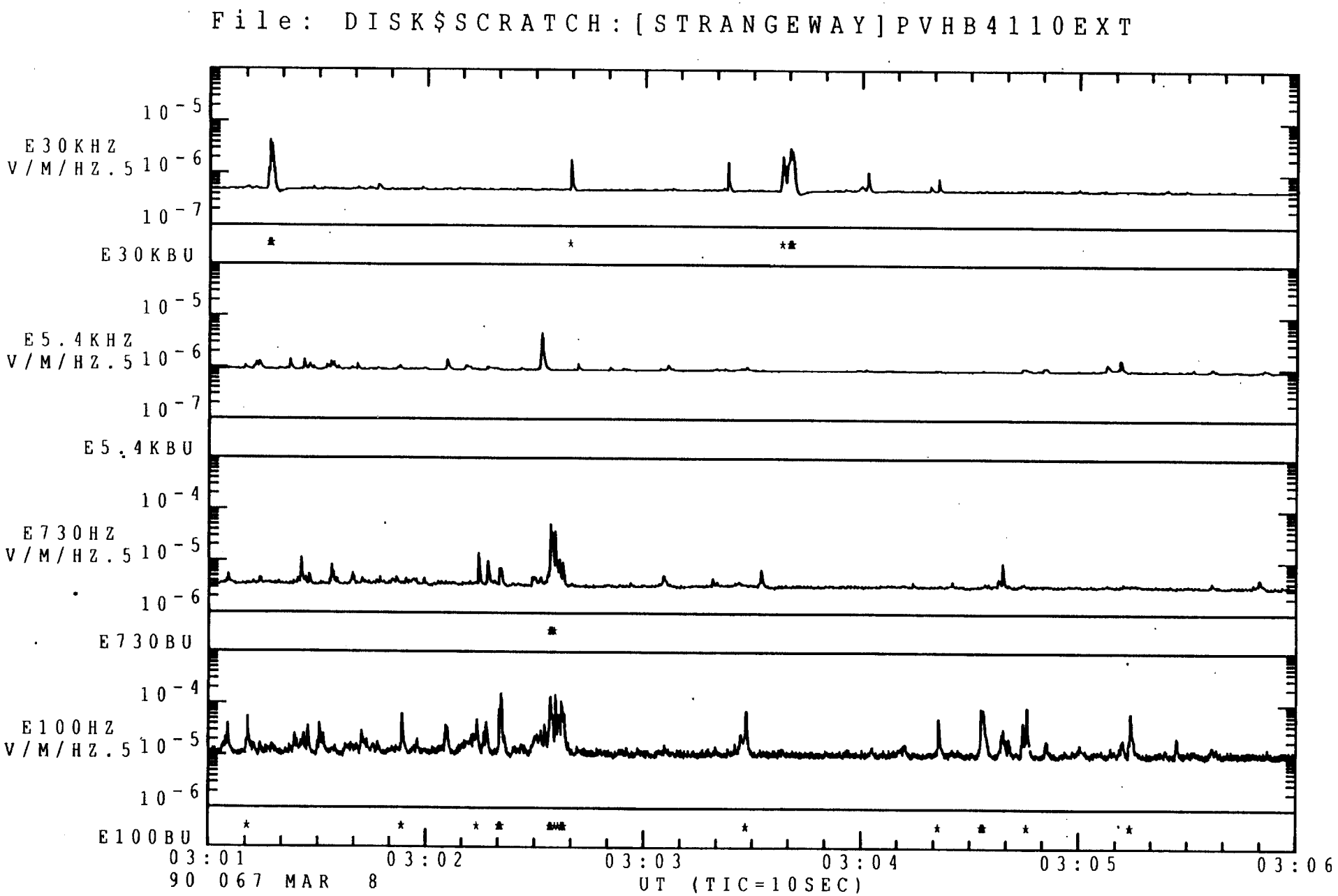
File: DISK$SCRATCH:[STRANGEWAY]PVHB4110EXT
E30KHZ V/M/HZ.5
10-5
10-6
10-7
E30KBU
E5.4KHZ V/M/HZ.5
10-5
10-6
10-7
E5.4KBU
E730HZ V/M/HZ.5
10-4
10-5
10-6
E730BU
E100HZ V/M/HZ.5
10-4
10-5
10-6
E100BU
03:01
03:02
03:03
03:04
03:05
03:06
90 067 MAR 8
UT (TIC=10SEC)

Figure 9

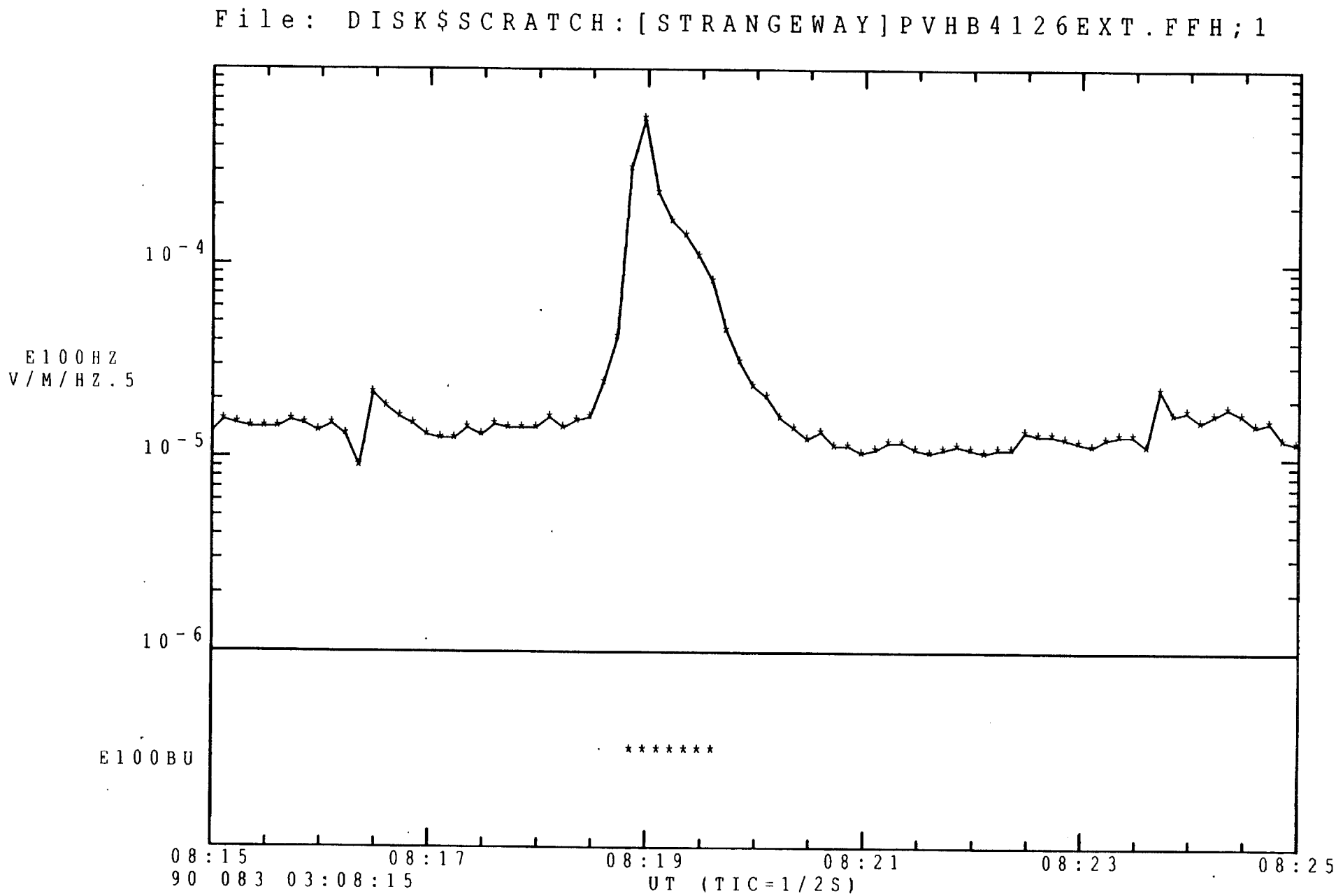
File: DISK$SCRATCH:[STRANGEWAY]PVHB4126EXT.FFH;1
E100HZ
V/M/HZ.5
10-4
10-5
10-6
E100BU
****
08:15
08:17
08:19
08:21
08:23
08:25
90 083 03:08:15
UT (TIC=1/2S)

Figure 10

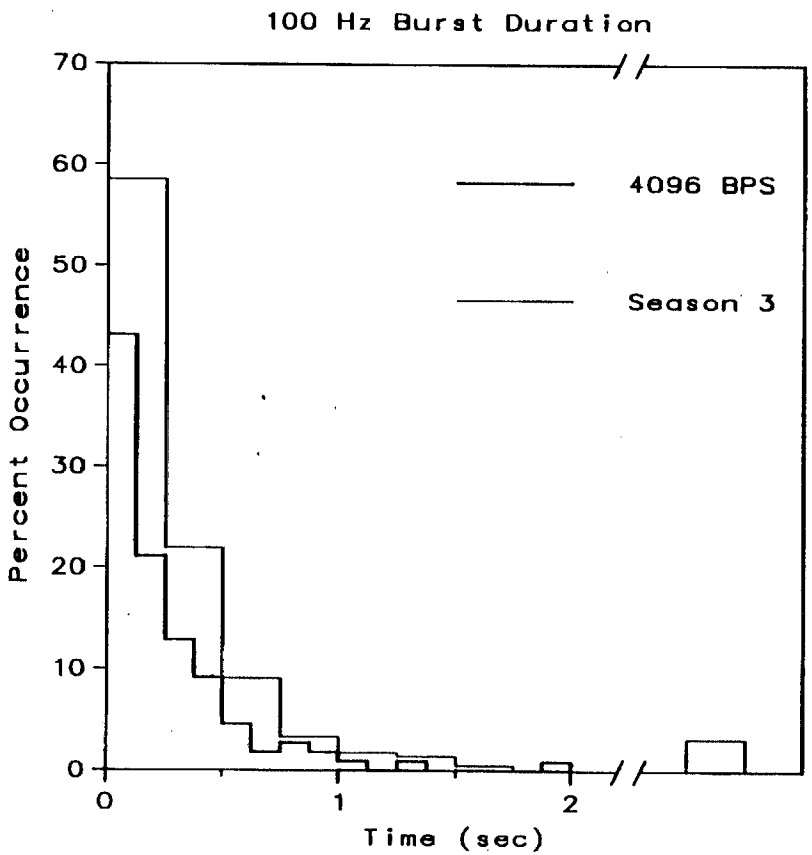
100 Hz Burst Duration
Percent Occurrence
70
60
50
40
30
20
10
0
0
1
2
Time (sec)
4096 BPS
Season 3

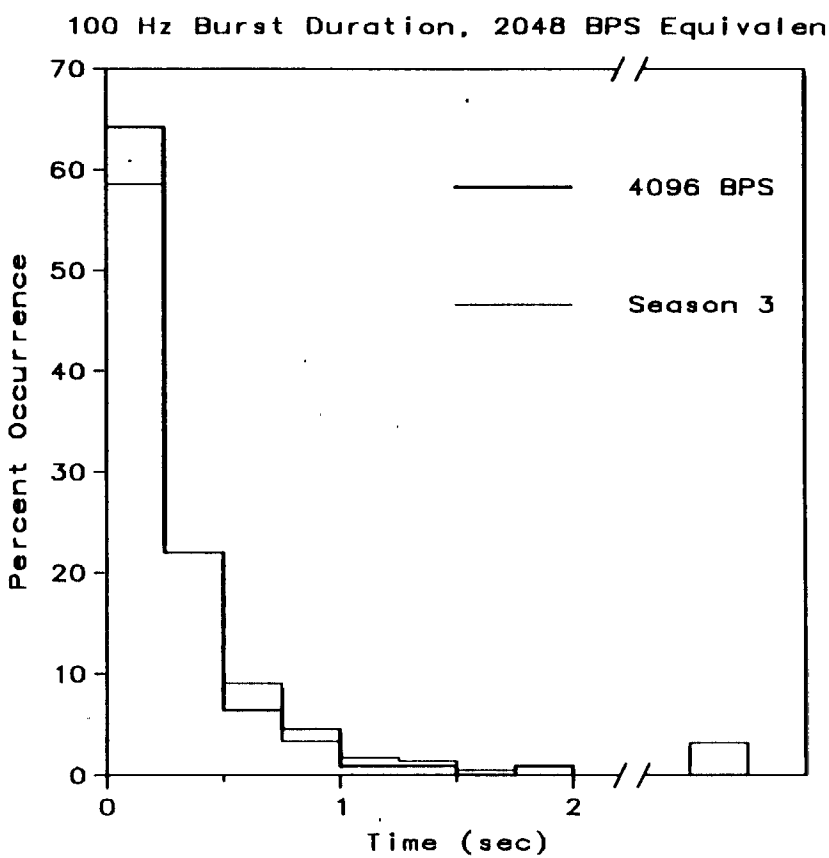
100 Hz Burst Duration, 2048 BPS Equivalent
Percent Occurrence
70
60
50
40
30
20
10
0
0
1
2
Time (sec)
4096 BPS
Season 3

Figure 11

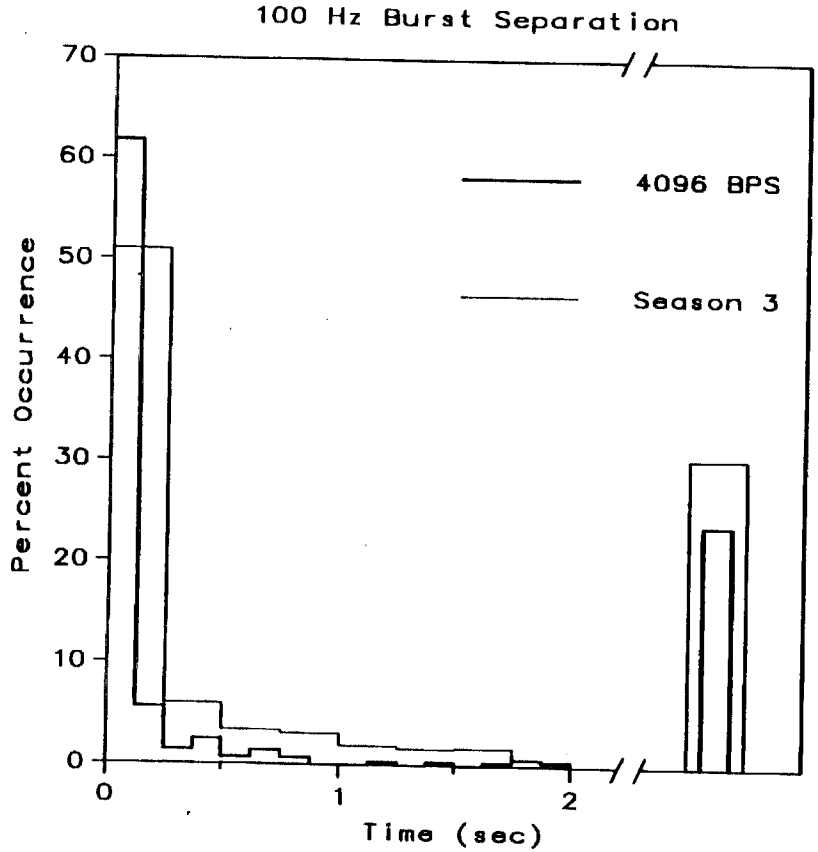
100 Hz Burst Separation
Percent Occurrence
70
60
50
40
30
20
10
0
0
1
2
Time (sec)
4096 BPS
Season 3

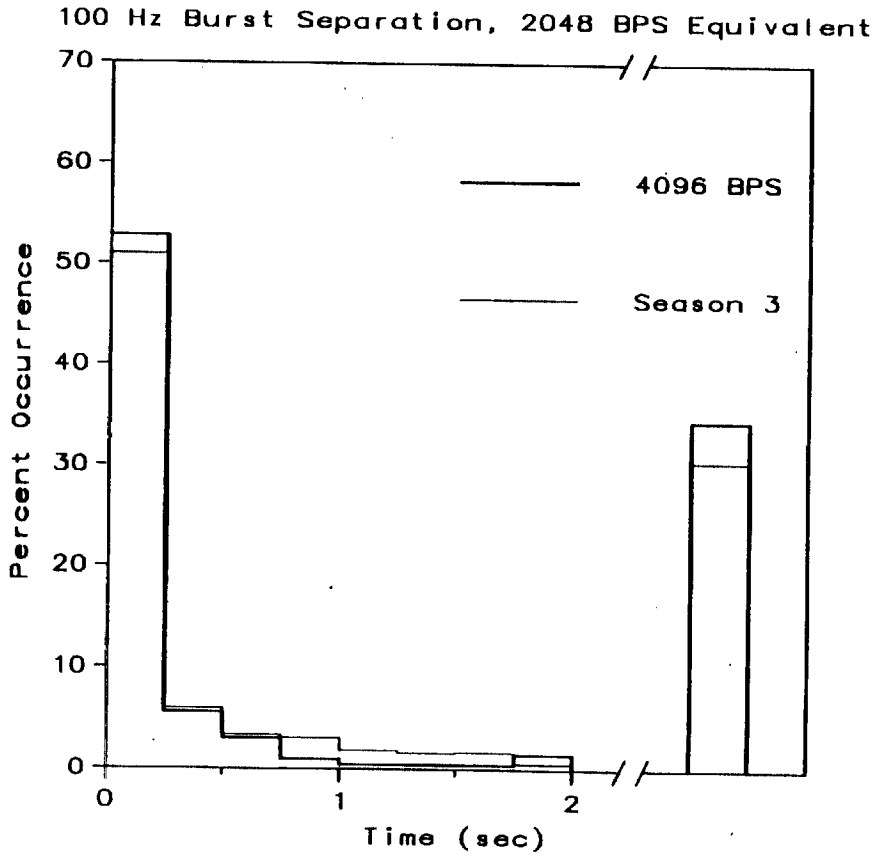
100 Hz Burst Separation, 2048 BPS Equivalent
Percent Occurrence
70
60
50
40
30
20
10
0
0
1
2
Time (sec)
4096 BPS
Season 3

Figure 12